1. SCIENTIFIC RESEARCH

1.1. CONDENSED MATTER PHYSICS

The main objectives of research in the framework of the theme involved the application of neutron scattering techniques and complementary methods to investigate the structure, dynamics and microscopic properties of nanosystems and novel materials, which are of great importance for the development of nanotechnologies in the fields of electronics, pharmacology, medicine, chemistry, modern condensed matter physics and interdisciplinary sciences.

The greater part of experimental research was carried out on spectrometers of the modernized IBR-2 reactor in accordance with the *Topical Plan* for *JINR* Research and International Cooperation and FLNP User Program. A number of scientific experiments were performed in neutron and synchrotron centers in Russia and abroad under the existing cooperation agreements and accepted beam time application proposals. Also, the activities on the modernization of the available spectrometers and the development of new instruments were carried out in accordance with the development program plan for the IBR-2 spectrometers. Most attention was given to the realization of the top-priority projects (construction of a new DN-6 diffractometer for studying microsamples and a multipurpose GRAINS reflectometer).

Within the framework of investigations under the theme the employees of the FLNP Department of Neutron Investigations of Condensed Matter (NICM) maintained broad cooperation with many scientific organizations in Russia and abroad. The cooperation, as a rule, was documented by joint protocols or agreements. In Russia, especially active collaboration was with the thematically-close organizations, such as RRC KI, PNPI, SSC RF IPPE, MSU, IMP UB RAS, IC RAS, INR RAS and others.

A list of the main scientific topics studied by the employees of the NICM Department includes:

- Investigation of structure and properties of novel crystal materials and nanosystems by neutron diffraction;
- Investigation of magnetic colloidal systems in bulk and at interfaces;
- Investigation of structure of carbon nanomaterials;
- Magnetism of layer nanostructures;
- Investigation of nano-scale structure and functional characteristics of biological, colloidal and polymeric nanodispersed materials;
- Investigation of nanostructure and properties of lipid membranes and lipid complexes;
- Investigation of atomic dynamics of nanosystems and materials by neutron inelastic scattering;
- Investigation of texture and properties of minerals and rocks;
- Analysis of internal stresses in bulky materials and factory-made goods.

1.1.1. Scientific results

1.1.1.1. Structure investigations of novel oxide, intermetallic and nanostructured materials

The crystal and magnetic structure of multiferroic $RbFe(MoO_4)_2$ has been studied by means of neutron and x-ray diffraction, as well as magnetic susceptibility measurements at pressures up to 10 GPa in a temperature range from 1.5 to 300 K [1] (**Fig. 1**). In this compound a spontaneous electric polarization occurs due to the fact that the inversion symmetry of the crystal structure is broken because of the occurrence of noncollinear antiferromagnetic ordering. In addition, Fe magnetic moments in the trigonal structure of $RbFe(MoO_4)_2$ (space group P-3m1) form a two-dimensional magnetic triangular lattice, where magnetic coupling between the magnetic planes is 25 times weaker than the in-plane coupling. With increasing pressure a structural phase transition to the monoclinic *C*2/*c* phase with a phase coexistence in a wide pressure range (residual fraction of the trigonal phase was present up to 10 GPa) was observed. The antiferromagnetic (AFM) symmetry for the trigonal phase is characterized by a propagation vector q = (1/3, 0, k_z). With a rise in pressure an increase in

the k_z value from 0.45 to 0.48 and in the Néel temperature with a pressure coefficient of 0.09 GPa^{-1} was observed. No evidence of the formation of the magnetic ordering in the high-pressure monoclinic phase was found down to the temperature of 1.5 K.

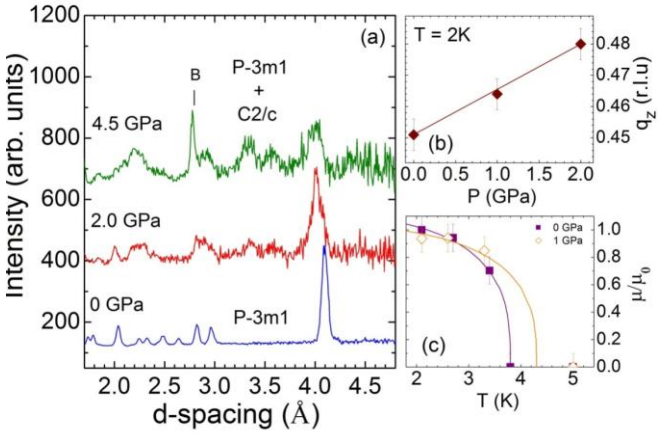

Fig. 1. Neutron diffraction patterns (DN-12 diffractometer, IBR-2) illustrating a structural phase transition in $RbFe(MoO_4)_2$ at high pressures (a). The sign "B" marks a peak from the anvils of a high-pressure cell. Pressure dependence of the k_z component of the propagation vector of the AFM structure (corresponding to the trigonal phase of $RbFe(MoO_4)_2$) determined at T = 2 K (b). Temperature dependences of the ordered Fe magnetic moment for the trigonal phase at various pressures, which are normalized to the value obtained at T = 2 K (c).

The studies of structural and magnetic phase transitions in $CuFe_2O_4$ copper ferrite have continued [2], **Fig. 2**. Additional neutron diffraction experiments have been carried out on a high-resolution powder diffractometer HRPT (SINQ, PSI, Switzerland). Copper ferrite crystallizes into a classical spinel structure and may exist in two symmetry modifications, cubic (sp. gr. *Fd*3*m*) at T > 700 K and tetragonal (sp. gr. *I*41/*amd*) below this temperature. The character of temperature changes in the interatomic spacing indicates that the structural transition is based on the Jahn–Teller distortion of CuO_6 octahedra rather than the mutual migration of copper and iron atoms. It has been established that cubic-to-tetragonal phase transitions are characterized by the equilibrium coexistence of both structural phases in a rather wide temperature range (~40°C). The characteristic sizes of the domains of coexisting phases are large (~1000 Å, mesoscopic phase separation). One of the reasons for stabilization of this phase is long-range internal stresses inside the crystallites, which develop during the structural phase transition and are reflected in a significant anisotropic broadening of diffraction peaks. The temperature of the formation of the ferromagnetic order is much higher (by ~50 K) than the temperature of the structural transition. This is an indication of a weak interaction between lattice (orbital) and magnetic (spin) subsystems. Lack of the relationship between structural and magnetic transitions in $CuFe_2O_4$ is one of the major differences of this spinel from normal spinels with magnetic cations only in B-sites, in which due to the formation of a "pyrochlore lattice" by magnetic atoms the long-range magnetic order is formed only because of the weakening of frustrations in the structural phase transition.

On the HRFD diffractometer the investigations of electrodes in lithium-ion accumulators [3] have continued. In-situ neutron diffraction experiments have been carried out to study charging-discharging processes of commercial lithium accumulators with $LiFePO_4$ (LFP) and graphite electrodes in real time. The experimental data have made it possible to follow more closely the stages of Li intercalation into graphite with the successive formation of several LiC_n phases and a reversible transition $LiFePO_4 \leftrightarrow FePO_4$. The comparison of charging/discharging processes in batteries with a cathode of pure LFP and LFP containing ~ 1% vanadium (LFPV) has demonstrated that in the latter case significantly greater fraction of the anode material undergoes a transition into a final LiC_6 phase because of a smaller relative mass of graphite as compared to fluorine ferrophosphate. The analysis of changes in the microstructure of a vanadium-doped cathode has shown a significant increase in the degree of structure imperfection, which correlates with the best electrochemical properties of LFPV as compared to LFP.

1. SCIENTIFIC RESEARCH

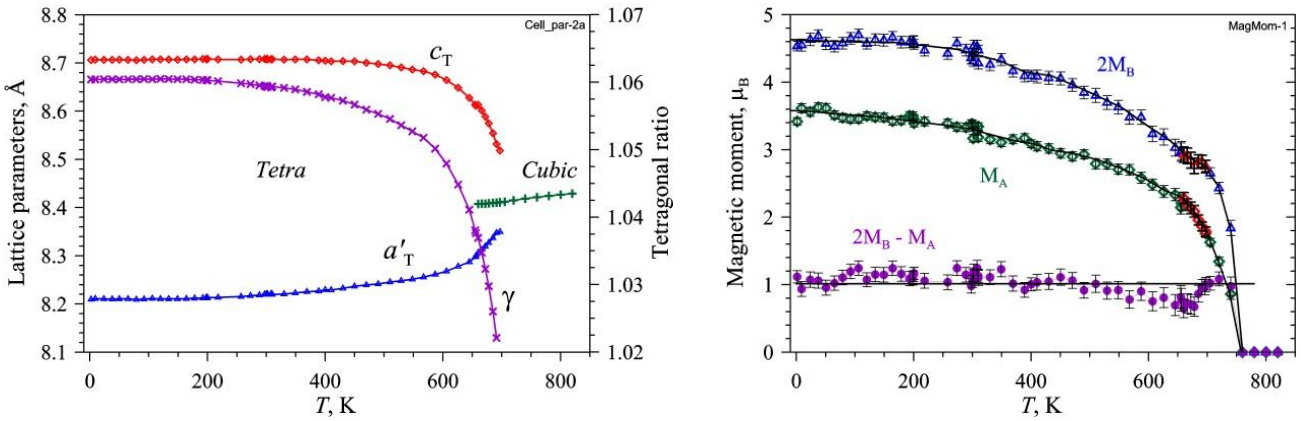

Fig. 2. Left: Temperature dependences of the unit-cell parameters of the cubic and tetragonal phase (left scale) and the tetragonal ratio (γ, right scale). The parameter $a'_T = \sqrt{2}\cdot a_T$ in the tetragonal phase is shown for the sake of visual convenience. Some temperature points were measured twice. The statistical errors are smaller than the symbol sizes. Right: Temperature dependences (data were obtained on heating) of the ordered magnetic moment in octahedral (doubled value, $2M_B$) and tetrahedral (M_A) sites and their difference ($2M_B$ - M_A). The statistical errors are given. The lines through $2M_B$ and M_A points are drawn for visual convenience. The line drawn through their difference is an average (1.01 μ_B) of all points in the range from 1.5 to 750 K.

On the DN-12 diffractometer the crystal and magnetic structure of intermetallic cobalt compounds RCo_2 (R = Tb, Ho) has been studied in a pressure range of up to 5 GPa [4], **Fig. 3**. In these compounds, unusual physical phenomena have been found, among which is a transition from nonmagnetic to a magnetically ordered state of the cobalt sublattice under changes of ionic radius and magnetic moment of R-cation. It has been established that in $TbCo_2$ under pressure there is a sharp linear decrease in the Curie temperature with a pressure coefficient of −9 K/GPa and in the ordered magnetic moment with a coefficient of −0.1 μ_B/GPa.

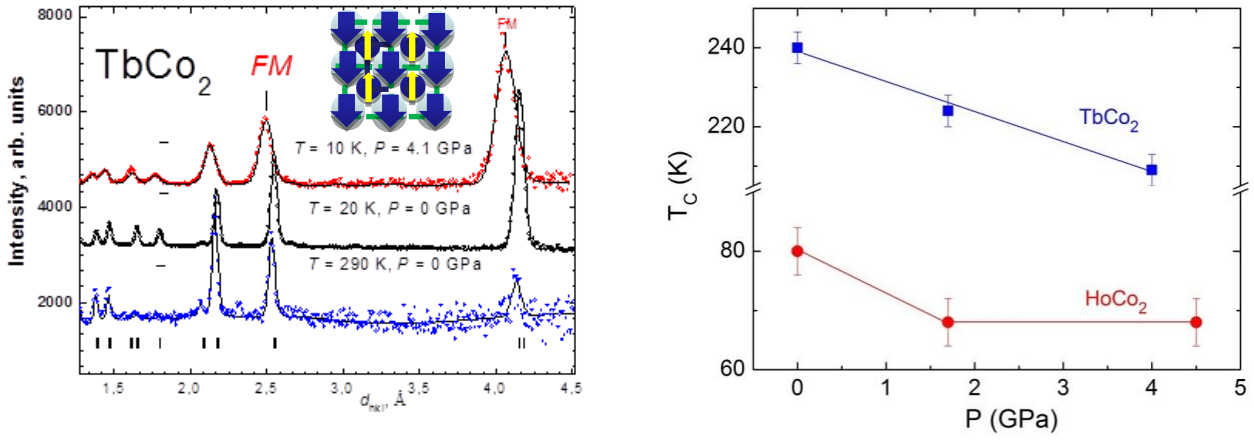

Fig. 3. Left: Neutron diffraction spectra of $TbCo_2$ obtained at various pressures and temperatures on the DN-12 diffractometer. The “FM” signs indicate peaks with the largest magnetic contribution from the ferrimagnetic ordering of Tb and Co sublattices. Right: Pressure dependences of the Curie temperature in $TbCo_2$ and $HoCo_2$.

At the same time the Tb ordered magnetic moment does not vary with pressure. In $HoCo_2$ the change in the Curie temperature has a nonlinear character; in the range of 0-1.7 GPa its decrease is

characterized by a pressure coefficient of –6 K/GPa, at higher pressures it weakly depends on pressure. The ordered magnetic moment in this compound decreases under pressure with approximately the same coefficient as in $TbCo_2$ (–0.1 μ_B/GPa).

On the DN-6 diffractometer the crystal structure of a double perovskite antiferroelectric Pb_2MgWO_6 has been studied under high pressures up to 5.4 GPa and at room temperature (**Fig. 4**). A structural phase transition from an orthorhombic antiferroelectric phase with *Pnma* symmetry to a cubic paraelectric phase with *Fm-3m* symmetry has been observed at $P \sim 1$ GPa. Structural parameters of both phases and their pressure dependences have been determined.

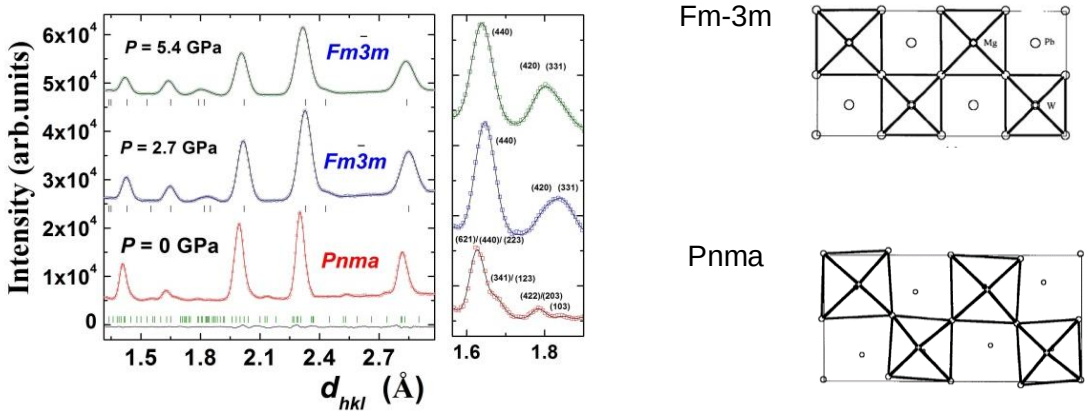

Fig. 4. Left: Neutron diffraction spectra of Pb_2MgWO_6 obtained at different pressures. Right: Schematic representation of the crystal structure of the orthorhombic antiferroelectric phase with *Pnma* symmetry and cubic paraelectric phase with *Fm-3m* symmetry.

The investigations of structural features and luminescent properties of crystal phosphors based on lutetium aluminum garnets $Lu_3Al_5O_{12}:Ce^{3+}$ doped with Lu_2O_3 nanoparticles have continued. It has been found that in the process of heat treatment no new structural phases are formed in this system, however the formation of a stable defect region occurs at the phase interface between LuAG:Ce and Lu_2O_3, which is evidenced by a change in all structural characteristics of LuAG:Ce after doping with lutetium oxide.

1.1.1.2. Investigation of magnetic fluids and nanoparticles

The experimental aspects of the observation of particle interaction effects in polydisperse magnetic fluids by means of small-angle neutron and X-ray scattering have been considered [5]. Various interaction regimes predicted by the theory of dipolar fluids with respect to the analysis of the scattering structure-factor under different conditions (with and without external magnetic fields) have been studied. It has been found that for adequate verification of the theory the corresponding experimental studies should be focused on a detailed analysis of the low-coupling regime (low dipole interaction constant, high particle concentration) in the case of magnetic fluids with hard and soft stabilizing shells. From this viewpoint the comparison of the experimental scattering data for magnetic fluids stabilized with various methods has shown that classical magnetic fluids based on non-polar organic solvents with magnetite nanoparticles (characteristic size 8 - 10 nm) stabilized by oleic acid are the most informative systems. The chain-formation regime (high dipole interaction constant, low particle concentration) has been discussed as well. Its analysis by small-angle scattering is significantly easier than the low-coupling regime. Actually, any magnetic fluid in this regime can be represented as a two-phase solution comprising non-interacting aggregates and separate particles. However, this regime seems to be difficult to realize in practice because of the accompanying non-equilibrium aggregation of strongly interacting magnetic nanoparticles during the preparation of

magnetic fluids. Additionally, magnetic correlations of a specific type have been experimentally found in polydisperse magnetic fluids. They correspond to a rather strong effective repulsion in concentrated systems (volume fraction of magnetic material ~ 10 %) and, in contrast to the correlations in particle locations, also take place in diluted solutions (volume fraction of magnetic material ~ 1 %).

A detailed study of aqueous solutions of magnetoferritin (artificial biological complex based on apoferritin with various content of magnetic materials in the protein cavity) which are of current interest from a biomedical viewpoint has continued. Using the data of small-angle scattering of synchrotron radiation and neutrons (including the contrast variation) it has been found that even for relatively low loading factors of magnetic material (magnetite with 100-200 atoms of iron per apoferritin molecule) a partial destruction of the protein shell takes place (**Fig. 5**). It has been shown that this effect is stronger for higher loading factors. Additionally some aggregation of the complexes has been observed for high (> 500) loading factors.

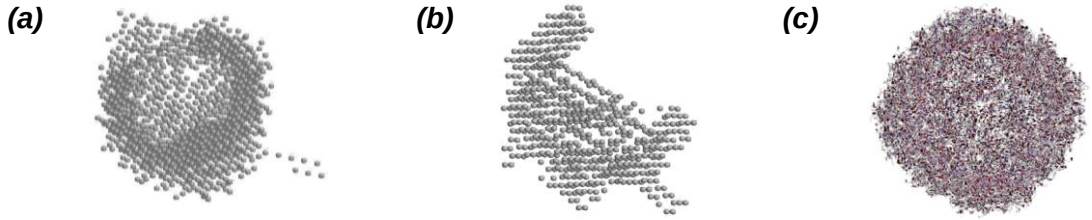

Fig. 5. Results of modelling based on experimental data of small-angle scattering from apoferritin (a); protein component in magnetoferritin with the loading factor LF = 156 (*b*) and comparison with the crystallographic data of apoferritin (*c*).

Small-angle neutron scattering has been applied along with the molecular dynamic simulations to study the interaction between solvents and saturated mono-carboxylic acids used in the stabilization of magnetic nanoparticles in ferrofluids based on non-polar organic solvents [6]. The scattering length density (SLD) distributions around acid molecules have been obtained with the help of molecular dynamics. The found modulation of these distributions depending on the acid length is consistent with the data of small-angle scattering from low-concentrated solutions on deuterated solvents. In particular, the use of the calculated SLD distributions makes it possible to describe fully the experimental scattering curves including residual incoherent background (**Fig. 6**).

The analysis of the neutron reflectometry data for the interface between a magnetic fluid (magnetite/sodium oleate/D_2O) and silicon has been performed. A strong contribution of the background diffuse scattering caused mainly by small-angle scattering from nanoparticles in the magnetic fluid adsorbed on the silicon surface has been observed. Several ways to take the background into account during the extraction of the specular reflection curve from experimental data have been studied [7]. From the comparison of the structural features of the magnetic fluid at the interface and in the bulk (small-angle scattering data) it has been concluded that separate particles are preferentially adsorbed on the silicon surface compared to their aggregates.

The behavior of polyethylene glycol (polymer introduced into the structure of aqueous magnetic fluids for increasing their biocompatibility) of low molecular mass (M_w = 400, 1000) in heavy water has been investigated using small-angle neutron scattering [8]. It has been shown that in concentrated solutions the polymeric molecules are partially associated into aggregates with the size of above 30 nm. The scattering from low concentrated solutions (< 3%) is indicative of the “Gaussian coil” conformation of the polymer; the corresponding form-factor (calculated by the Debye formula) has been used in the analysis of the scattering from concentrated solutions, which is well described by the model of “interacting Gaussian coils”.

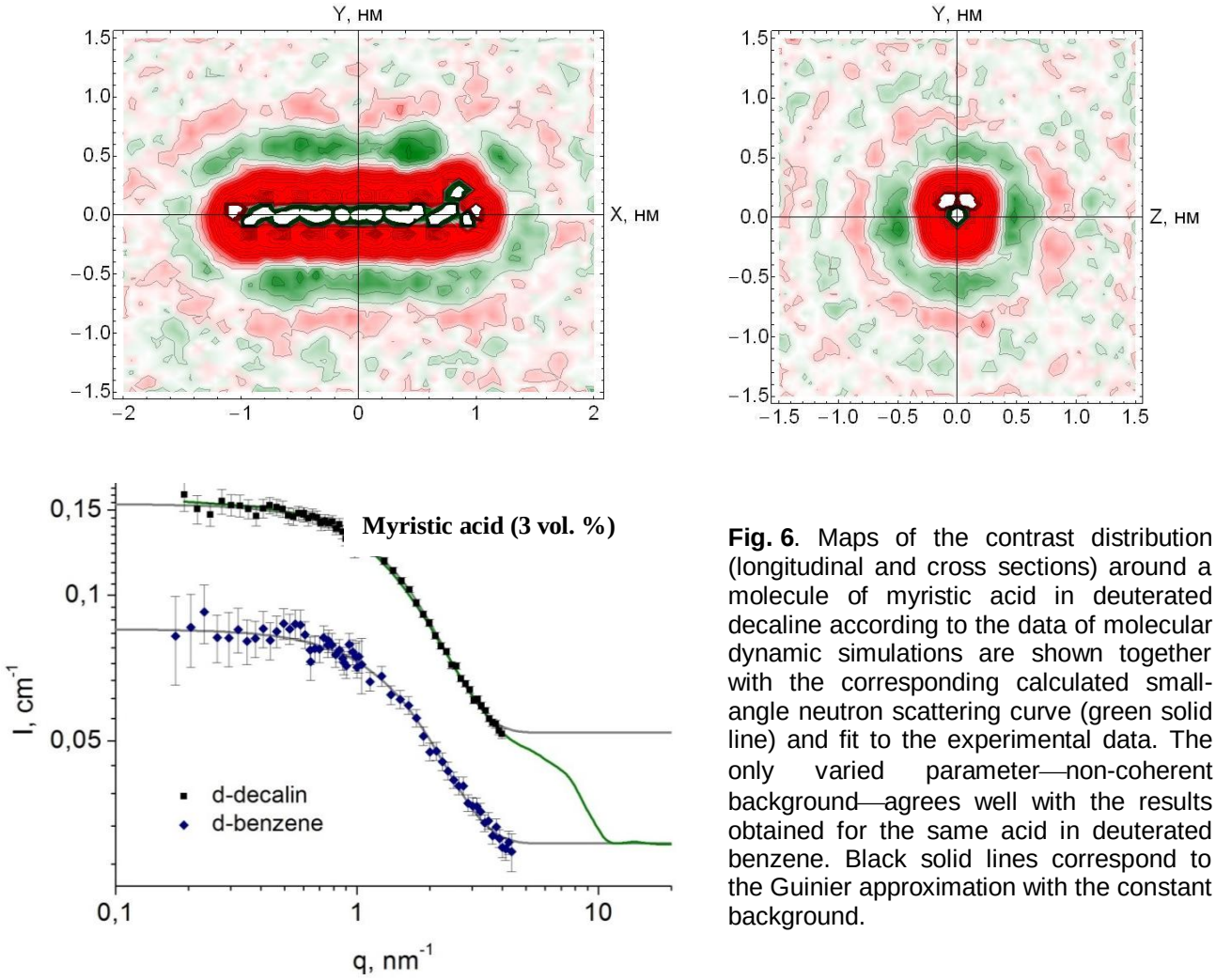

Fig. 6. Maps of the contrast distribution (longitudinal and cross sections) around a molecule of myristic acid in deuterated decaline according to the data of molecular dynamic simulations are shown together with the corresponding calculated small-angle neutron scattering curve (green solid line) and fit to the experimental data. The only varied parameter—non-coherent background—agrees well with the results obtained for the same acid in deuterated benzene. Black solid lines correspond to the Guinier approximation with the constant background.

1.1.1.3. Investigations of carbon nanomaterials

On the basis of the small-angle neutron scattering analysis (including the contrast variation) from liquid dispersions of detonation nanodiamonds (DND) a continuous spatial transition of the carbon state from crystalline diamond (sp^3-hibridization) inside the particle to a graphite-like state (sp^2-hibridization) at DND surface has been suggested (**Fig. 7**).

Such a transition makes it possible to combine the experimentally observed shift in the mean scattering length density of DND as compared to pure diamond (which is indicative of the presence of a non-diamond component in the DND structure) and the diffusive character of the particle surface, which can be deduced from the deviation from Porod's law [9]. The proposed profile is of a simple power-law type and due to a number of specific features explains a homogeneous decrease in the total scattering intensity at the contrast variation. A spherical 'core-shell' representation of DND particles used previously, which gives a reasonable thickness of a non-diamond shell of about 0.5 nm, can be considered as an approximation to the continuous density profile reflecting naturally the diamond-graphite transition in terms of the averaged scattering length density. Along with it, this profile naturally suggests that non-diamond transitional bonds (presumably sp^{2+x}-bonds) are mainly concentrated close to the particle surface. It also allows one to directly determine the parameters of the particle size distribution function.

1. SCIENTIFIC RESEARCH

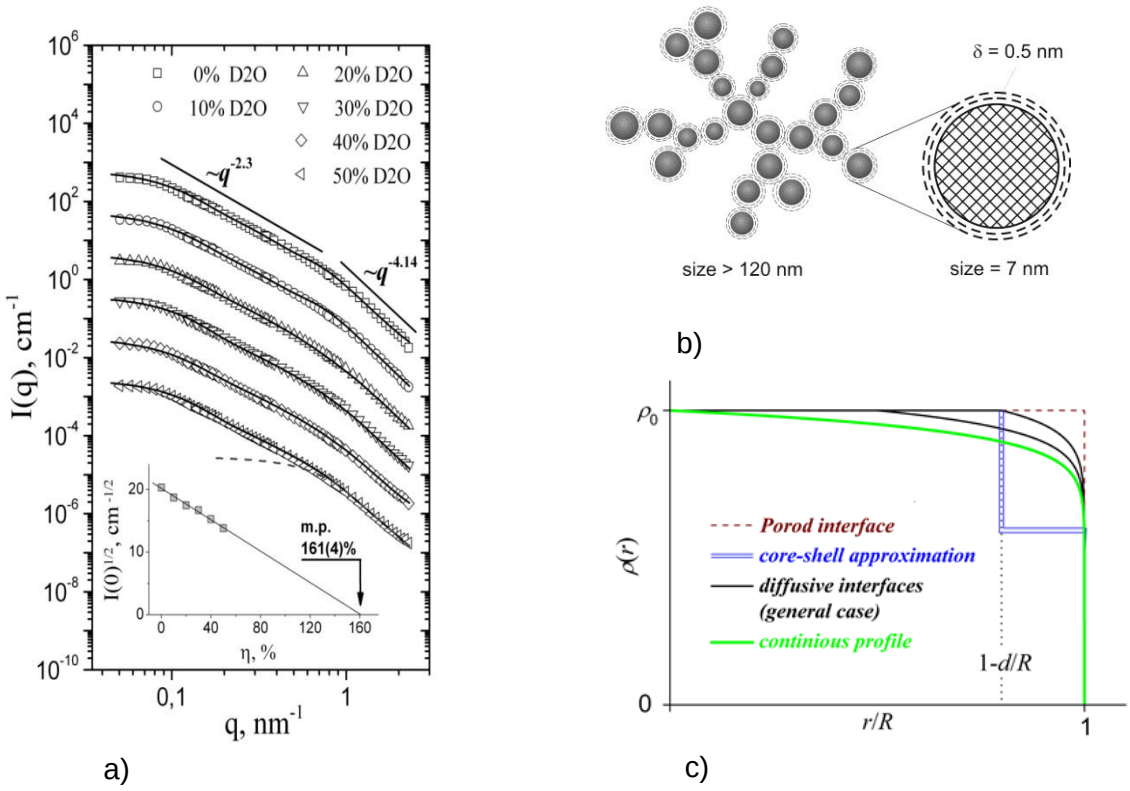

Fig. 7. Experimental curves of small-angle neutron scattering from liquid dispersions of detonation nanodiamonds (DNA) measured with the contrast variation (a). A schematic view of a DNS cluster in liquid dispersions with an enlarged schematic representation of its basic structural unit—a particle composed of crystalline diamond and graphene shell (b). Various approximations to this shell are considered. A continuous diffusive profile (green solid line) gives the best fits to the experimental curves (c).

A comparative structural characterization of fullerene C_{60} and C_{70} clusters in water and mixed solvent NMP/H_2O has been performed using small-angle neutron scattering. The aqueous solutions were synthesized by the solvent substitution method. To prepare the aqueous-organic system C_{60}/NMP/H_2O, fullerenes were initially dissolved in the organic solvent followed by the addition of water in such a proportion that the final volume fraction of NMP in the solutions did not exceed 0.005%. The size distribution function of the clusters was found for all samples. The possibilities for using NMP/H_2O-based fullerene solutions in biomedical applications were studied from the viewpoint of toxicity. In particular, the dependence of cytotoxicity of the solutions on the fullerene cluster size in them was of special interest [10].

1.1.1.4. Investigations of magnetic nanostructures

At the REMUR spectrometer the magnetic state of the layer nanostructure Ta(10nm)/V(150nm)/$Fe_{0.7}V_{0.3}$(1nm)/V(1.2nm)/$Fe_{0.7}V_{0.3}$/Nb(150nm)/Si composed of ferromagnetic and superconducting layers has been studied by polarized neutron reflectometry (**Fig. 8**). Three phenomena were supposed to take place in this nanostructure. The first one was assumed to be an antiferromagnetic ordering of the pair of $Fe_{0.7}V_{0.3}$(1 nm) layers in an external magnetic field. It must have been accompanied by an increase in the degree of antiferromagnetism during the superconducting transition of niobium (T_c=8.5K) and vanadium (4.8K) layers. The second effect was supposed to concern the magnetization of the superconducting pair by ferromagnetic layers, which

would result in magnetization of the superconducting layer. Finally, the third phenomenon was presumed to be the formation of a domain structure with small domain sizes and zero mean magnetization.

During the measurements the temperature and magnetic field strength were varied in the ranges of 1.3-110 K and 30 Oe - 9.5 кOe, respectively. The neutron scattering with a maximum at a temperature of 8K (which is below the temperature of superconducting transition in the niobium layer) was observed in the range of 1.3-10 K. The scattering was detected by a decrease in the neutron intensities of the specular reflected and refracted beams and by an increase in the neutron intensities at certain angles in a vertical plane (modes of small-angle scattering and grazing incidence small-angle scattering (**Fig. 8**)).

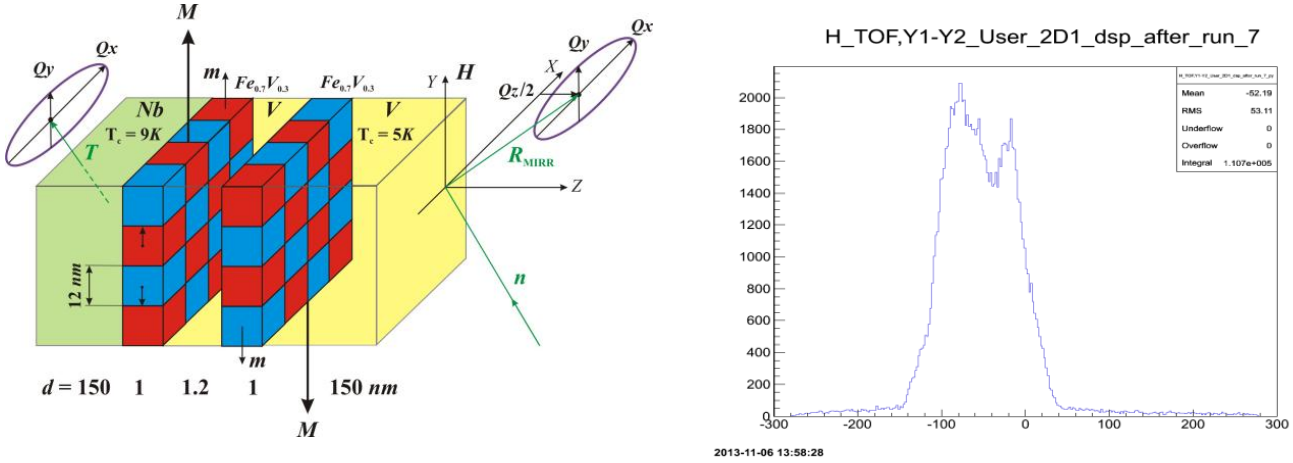

Fig. 8. At the left: Schematic representation of a cryptoferromagnetic state. At the right: Intensity of the beam of polarized neutrons (wavelength 1.29 ± 0.01 Å, incident grazing angle 5.4 mrad) transmitted through a sample as a function of the detector channel (vertical direction). Neutron diffraction peaks from a domain lattice (interplanar distance 50 nm) with a linear domain size of 12 nm are seen.

For the magnetic domain size the value of d = 12 nm was obtained at 8 K. The direction of the domain magnetic moments was varied periodically at the linear scale of L_1 = 43 nm (the scale of antiferromagnetic ordering) and L_2 = 87 nm. With lowering temperature L_1 decreased, while L_2 increased. At the magnetic field of 2.5 кOe, i.e. in the presence of magnetic anisotropy, the antiferromagnetic ordering occurred in pairs of nearest-neighbor domains (d = 11 nm, L_1 = 22 nm).

The obtained experimental data are indicative of the existence (in a certain temperature range below the superconducting transition temperature) of a domain lattice phase where a rotation of the magnetization vector takes place and which is characterized by two directions. The latter is testified by a strong scattering, which cannot be explained only by the scattering in the vertical direction. The absence of neutron scattering in the second direction suggests that the lattice constant in this direction lies in the range below one thousand angstroms.

These observations are the first direct experimental evidence of a cryptoferromagnetic phase in superconducting ferromagnetics, which is the appearance of an antiferromagnetic ordering at the scale of superconducting coherent length (size of a superconducting pair). At the same time, the magnetic period of the cryptoferromagnetic state was found to be an order of 1000 times less than the size of usual domains in ferromagnetics (microns).

At the REMUR spectrometer a layer structure 12×[Fe(35Å)Cr(4.4Å)/Gd(50Å)] where the exchange coupling between RE and PM ferromagnetics was regulated by a chromium layer, has been studied. It has been found that at room temperature (above the Curie temperature of bulk

gadolinium) there is a magnetic moment in gadolinium in the near-surface region close to interlayer boundaries and the magnetic moments of gadolinium and iron layers have opposite signs with respect to the direction of the magnetic field.

The ferromagnetic multilayer nanostructures of the Fe/MgO/Fe type, where magnetic layers are separated from each other by nonmagnetic layers, have been studied. These systems characterized by the giant magnetoresistance (GMR) effect are of current interest from the technological and scientific viewpoints, since they can be used as elements of spintronic devices. The GMR effect is provided by the tunneling of electrons between Fe-layers through a dielectric MgO-layer. The thickness of the latter influences the tunneling of electrons, which are involved in the exchange coupling between ferromagnetic layers, and thus changes the magnetic properties of the structure. The so-called spin valves based on a thin film structure MgO//Fe(200Å)/MgO(15Å)/Fe(50Å)/Ta(50Å) have been investigated. Principal characteristics of these systems are specific features in the hysteresis loop in the form of ledges (**Fig. 9**). The reflectivity has been measured in the fields corresponding to the specific points in the hysteresis curve. The measurements have shown good quality of the prepared samples and revealed an interesting magnetic behavior as a result of competition between Zeeman interaction, layer exchange coupling and magnetic anisotropy inside the iron layers.

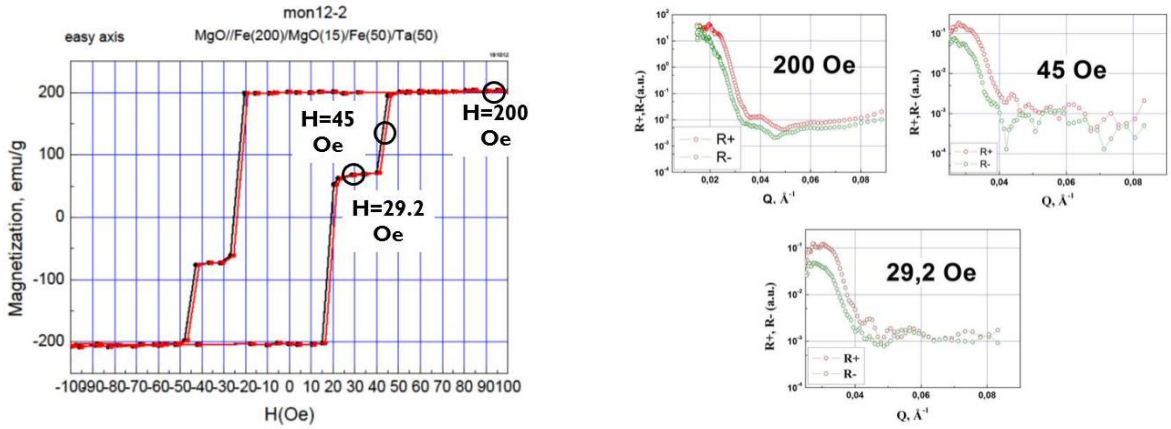

Fig. 9. Left: magnetization curve for the structure MgO//Fe(200Å)/MgO(15Å)/Fe(50Å)/Ta(50Å) in the external magnetic field directed along the easy axis. The open circles are the points where reflectivity has been measured. Right: obtained reflectivity curves.

1.1.1.5. Biological nanosystems, lipid membranes and complexes

A process of spontaneous phospholipid vesicle formation in the presence of calcium ions has been studied by small-angle neutron scattering (**Fig. 10**). For the first time, the behavior of intermembrane distance in the transition region has been considered in detail for the membranes in both liquid and gel phases. It has been shown that the transition of the system from the bound to the unbound state in both phases has a continuous character, which is rather unusual for gel phases. The earlier theoretical studies on gel phases suggested that on addition of calcium ions to lipid multilayer membranes there should be a sharp transition of membranes from the bound to the unbound state, since there are no undulations in the gel phase (membranes are 'harder' than in the liquid phase). The investigations performed have shown that there is a significant contribution of undulation forces into membrane interactions. The critical calcium ion concentrations at which the studied transition takes place in gel (0.3 mM) and liquid (0.4 mM) phases have been obtained together with the direct determination of the affinity constants for calcium ions with respect to lipid membranes (22 M-1 and 24 M-1 in gel and liquid phases, respectively).

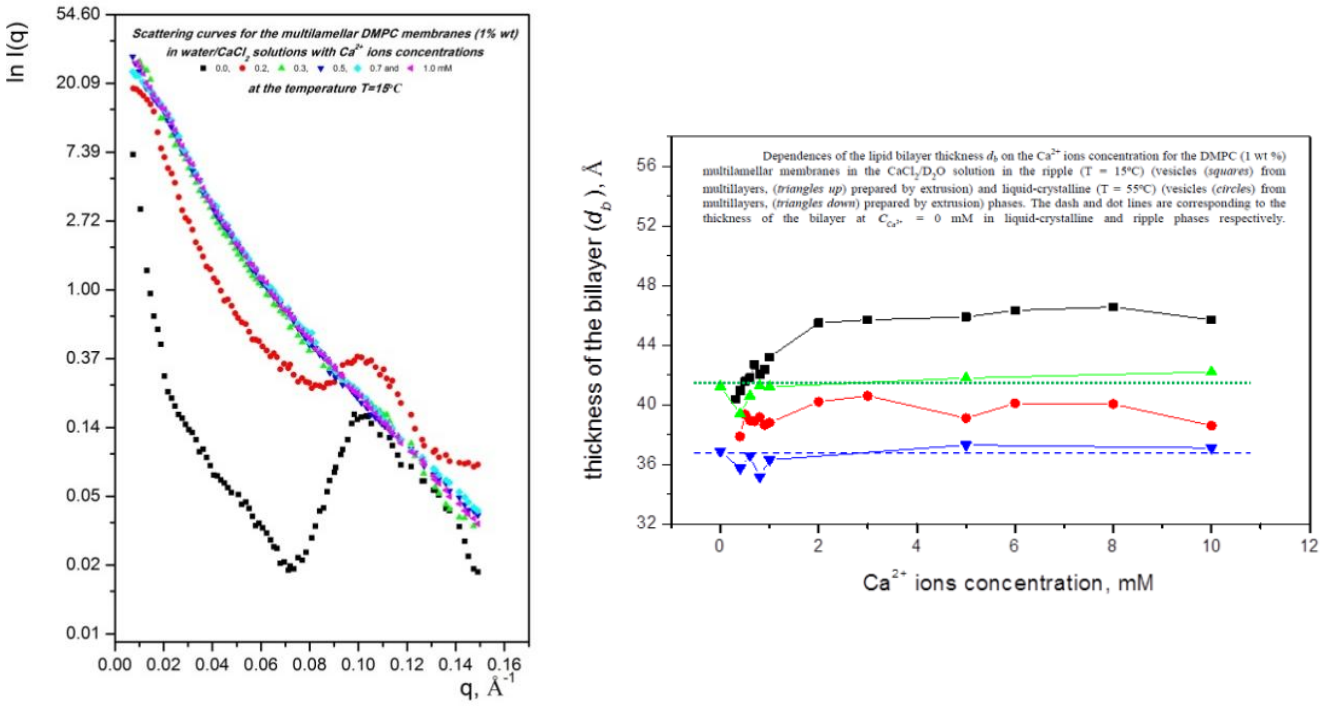

Fig. 10. Left: small-angle neutron scattering curves from multilayer membranes DMPC (1% wt) in the solution water/$CaCl_2$ for molar concentrations of Ca2+ ions: 0.0, 0.2, 0.3, 0.5, 0.7 1.0 mM. Right: concentration dependence of the bilayer thickness in different phases.

The packing of inner membranes (crista) from rat heart mitochondria has been investigated. This type of mitochondria is exposed to greater loads and has larger area of inner membrane as compared with mitochondria from liver studied previously. The diffraction peaks have been observed in the scattering curves, which can be related to the regular positioning of the inner mitochondrial membrane (structure parameter 200 Å). The osmotic shock applied to mitochondria and a priori destroying their structure has resulted in the suppression of the observed peaks. This supports the connection between diffraction peaks and the packing of the inner membrane. Using contrast variation the scattering curves have been obtained separately for protein and lipid components of mitochondria. It has been shown that the peaks appear mainly due to lipid bilayers. Also, it has been found that the inner membrane organization is sensitive to the tonicity of the environment and the presence of calcium ions. Calcium and tonicity of the environment play important roles in mitochondrial and cell signaling.

The development of methods for studying the structure of membrane proteins using small-angle neutron scattering has been started. The solutions of bicelles with a 'built-in' protein (bacteriorhodopsin) have been chosen as a system. At the moment a procedure for preparing becelles and incorporating the membrane protein in them has been developed. The information on the structure and behavior of bicelles in various conditions (temperature, concentration, lipid composition, presence of protein) has been obtained with the help of small-angle scattering.

The investigations of the structural features of connexin (protein) have been started using small-angle neutron and X-ray scattering from the solutions of different parts of the protein. Connexins are selective channels, which play a central role in cell communication. Structural anomalies of the given protein cause serious heart diseases. Connexins are composed of membrane and water-soluble parts. The experiments have demonstrated that the water-soluble part of connexin is a dimer with an elongated shape. A linear polymer is used to stabilize solutions of the membrane part of

connexin. Using small-angle X-ray scattering data it has been revealed that the polymer forms a massive “coat” around the protein, which makes it rather difficult to obtain information only about the protein (without the polymer). The application of neutron scattering with contrast variation has turned out to be difficult, since the protein aggregates in the presence of heavy water.

The study of model systems for drug delivery continued [11]. Different aggregation states in the system 1,2-dipalmitoyl-sn-glycero-3-phosphatidylcholine/deoxycholate (DPPC/NaDC) have been investigated by small-angle neutron scattering and dynamic light scattering. It has been found that depending on the concentration of NaDC this system shows a wide spectra of supramolecular formations including ellipsoidal vesicles (1.5 mM NaDC), ribbon-like structures (3.5 mM NaDC), spherical mixed micelles (10 mM NaDC).

1.1.1.6. Polymeric materials

The structural features of new polymeric composite materials with iron nanoparticles (size from 10 to 100 nm) have been studied by atomic force microscopy and small-angle neutron scattering [12] (**Fig. 11**). These materials show unique mechanical and rheological properties, which vary significantly under magnetic fields. Thus, in the case of a homogeneous external magnetic field with the strength of 0.4 T the compression modulus changes by a factor of 100. Under sufficiently strong magnetic fields the samples behave as elastoplastic materials.

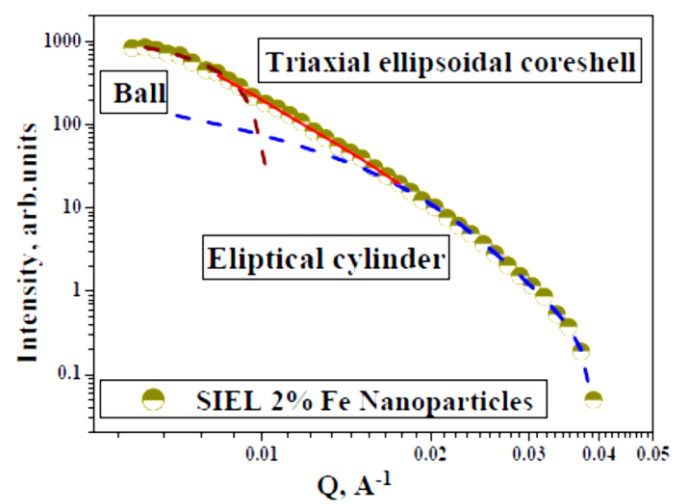

Fig. 11. Small-angle neutron scattering curve from a new polymeric composite material with iron nanoparticles.

In the framework of the study of the glass-transition kinetics in polymers the modeling of polystyrene vitrification has been performed in a wide range of cooling rates (10^{-4} - 2 K/s). The aim of the investigations was to determine the best model, which could describe experimental dependences of isobaric heat capacity in a temperature range of 90 - 130˚C. The Tool-Narayanaswami and Schmeltzer-Gutzov methods have been used as basic approaches. It has been shown that all existing approaches require a wide variation in the modeling parameters (as a minimum, parameter of non-exponentiality β) at different cooling rates. It has been concluded that the Schmeltzer-Gutzov method with an original expression for the relaxation time of the system, τ, is as good as other methods for describing qualitatively the experimental data of differential scanning calorimetry [10].

1.1.1.7. Atomic and molecular dynamics

An experimental and theoretical study of molecular dynamics and structure of derivative compounds alkylcoumarin-hexafluorophosphate (ESP-PF6) and tosylate (ESP-TOS) has been carried out (**Fig. 12**). The experimental investigation has been performed using infrared absorption spectroscopy, Raman scattering, inelastic neutron scattering and terahertz radiation.

The density functional theory approximation and software packages CASTEP and GAUSSIAN09 were used for theoretical modeling of molecular dynamics. The experimental data show good agreement with the results of theoretical modeling.

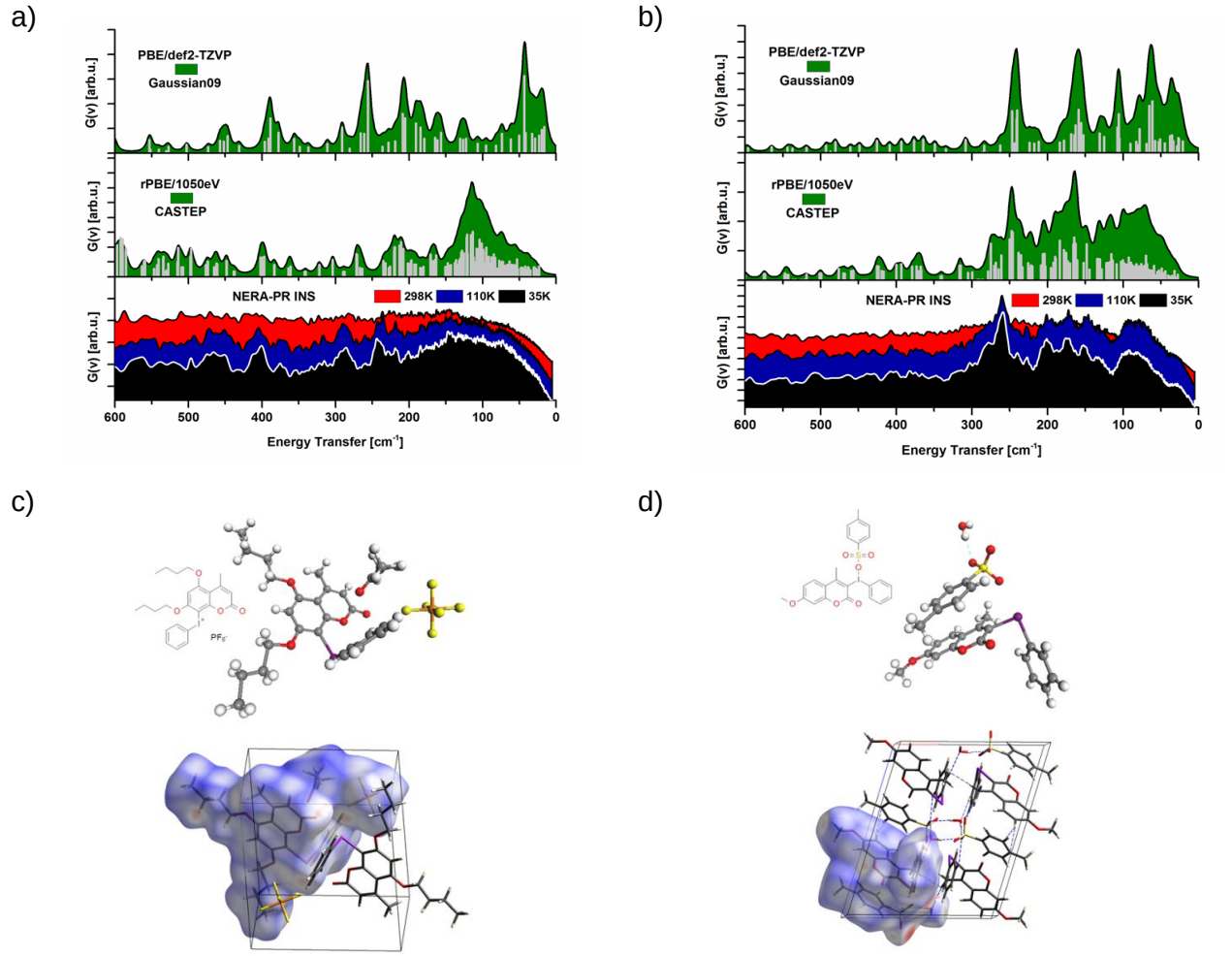

Fig. 12. Inelastic neutron scattering spectra; results of their theoretical modeling in the framework of various approximations and the crystal structure of ESP-PF6 (a,c) and ESP-TOS (b,d).

The atomic dynamics of liquid gallium has been studied at high temperatures using inelastic neutron scattering. A quasi-elastic part including both coherent and incoherent components was found from experimental double-differential scattering cross-sections of liquid gallium obtained at temperatures of 313, 433, 553 and 673 K. In the case of coherent scattering the analysis of the spectra was performed in the Q-range in the vicinity of the first structure factor maximum ($Q \sim Q_o$). A modified hard-sphere fluid model was used and a temperature dependence of self-diffusion coefficient for liquid gallium was obtained in the range of 313-673 K. For incoherent scattering the quasi-elastic data were analyzed in a wider Q-range and the obtained results were described by a simple diffusion model. The results of two methods of analysis are in good agreement with respect to both the diffusion coefficient value and its temperature dependence and are roughly described by the Arrhenius law with a constant energy of activation of ~ 6 kJ/mol. From the analysis of the shape of coherent and incoherent quasi-elastic scattering peaks it has also been found that the decay of density fluctuations of the immediate surrounding in liquid gallium follows a simple exponential law.

1. SCIENTIFIC RESEARCH

1.1.1.8. Applied research

Among traditional applied investigations in the NICM Department are the experimental studies of internal stresses and texture of rocks and minerals, determination of internal stresses in bulk materials and products, including engineering materials and components of machines and devices. For the most part, these investigations are carried out using neutron diffraction.

Control over a condition of metal of a reactor vessel during its service life and a guarantee of its integrity under normal operation conditions as well as in case of any design accidents is one of the key problems of the present-day nuclear power engineering. When operating nuclear facilities a surveillance program of witness specimens positioned at the inner wall of a reactor cavity serves as an important source of information on changes in properties of vessel steels, which tend to worsen as a result of neutron irradiation. To increase the number of irradiated samples of reactor vessel steel for validation of its design service life or for its extension, the technology of reconstitution of witness specimens after their mechanical tests using different types of welding (electric-arc, electron-beam, laser-beam, etc.) is used. This requires the level of residual stresses to be controlled after welding in the reconstituted witness specimens.

On the FSD diffractometer the experiments have been carried out to study the distribution of residual stresses in witness specimens that develop after electron-beam welding (EBW) and laser beam welding (LBW). The experimental results (**Fig. 13**) have shown that the level of residual stresses for an LBW sample is much higher than for an EBW sample and ranges to 550 MPa in the weld region.

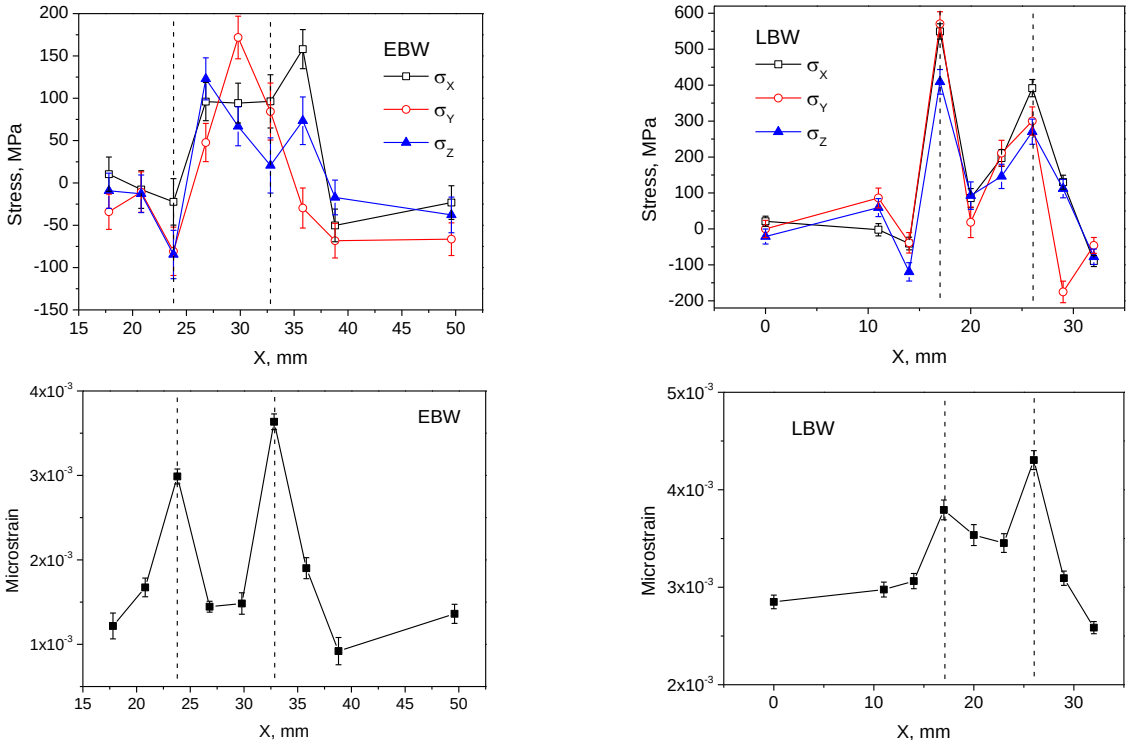

Fig. 13. Distribution of residual stresses (top) and microstrains (bottom) in samples reconstituted by electron- and laser-beam welding.

This supports the well-known fact that among all methods the application of electron-beam welding results in the lowest level of residual stresses in welds. This is most probably due to a low heat input of the EBW process (4-5 times lower than, for example, in arc welding) which significantly

reduces the deformation of a final product. In addition, the diffraction peak broadening was used to determine the level of residual microstrains, which directly characterizes the density of dislocations in a material being studied. The microstrain in the EBW specimen amounts to $3.5 \cdot 10^{-3}$ and is slightly higher in the LBW specimen – $4.5 \cdot 10^{-3}$. This effect is accompanied by a considerable (~ 2.5 times) increase in microhardness in weld seam regions. The observed increase in microhardness is likely to be the result of the formation of martensite (or martensite-bainite) structure in welds and heat-affected zones.

The investigation of residual stresses in calcite-based rock samples, which are induced by the presence of magnetic pyrrhotite has been conducted on the Epsilon diffractometer. The distribution of internal stresses in the calcite phase has been determined as a function of the angle of rotation of the sample in the XY plane around the Z axis.

The texture of a number of ferritic-pearlitic steel samples has been investigated with the aim of studying the effect of treatment, chemical composition and texture on the strength properties of railway car wheels made of this steel. On the basis of the measurement of pole figures (200), (110), (211) for α-Fe performed on the SKAT diffractometer it has been concluded that heat treatment destroys texture. Doping of the alloy results in the reorientation of weak preferred orientation.

The experiments have been carried out to study thermal internal stresses in marbles that are induced by seasonal temperature variations [15].

1.1.2. Instrument development

Work to develop and test sample environment devices for the new DN-6 diffractometer has been carried out. A cryostat for experiments with high-pressure cells has been constructed and tested. High-pressure cells with diamond anvils with an operating range up to 15 GPa (culet diameter of 0.8 mm) and 50 GPA (culet diameter of 0.5 mm) have been purchased. The first experiments have demonstrated a possibility of their successful application in experiments on DN-6. An advanced detector system has been designed for obtaining spectra at a scattering angle of 90° on the basis of 96 separate gas counters. The implementation of this system will allow a 3-4-fold increase in the neutron flux at the instrument.

The operation of the first-stage of the GRAINS reflectometer has started. Beam profiles have been measured and optimized for different configurations of the reflectometer elements. The experimental estimations of the total flux of non-polarized thermal neutrons (wavelength above 0.05 nm) after deflector have been made in thermal (2×10^6 cm^{-2} s^{-1}) and cold (1×10^6 cm^{-2} s^{-1}) operating modes of the moderator. Time-of-flight spectra have been optimized over the fast neutron background. The first reflectivity curves for standard systems have been obtained in two operating modes of the moderator (**Fig. 14**). During the start-up the first experiment to study the oxidation effect on the structure of thin titanium films on a glass substrate has been carried out in the framework of the development of new coatings for neutron optical devices.

The activities on the implementation of the project to develop and construct a new diffractometer on beam 6a for real-time neutron diffraction studies of transient processes have continued. Design drawings of background shielding for a detector system have been prepared. An adjustable neutron beam diaphragm providing linear movement along the horizontal and vertical axes and mounted on an outlet flange of the RTD neutron guide has been manufactured and installed.

a) *b*)

1. SCIENTIFIC RESEARCH

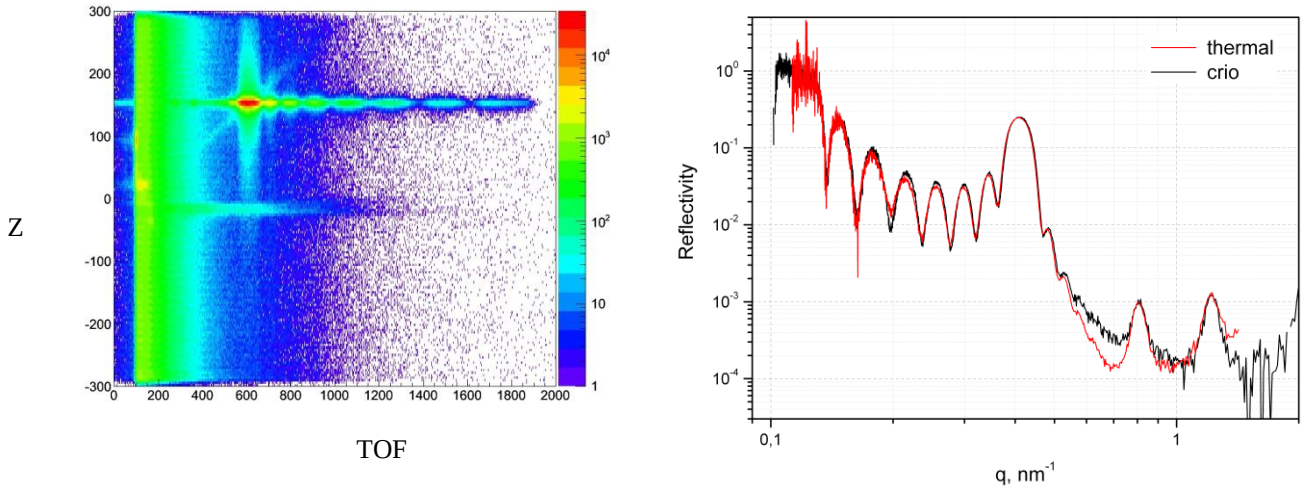

Fig. 14. a) 2D spectrum of non-polarized neutron beam reflected from a layer structure [Ni(8.4nm)Ti(7nm)]×8/Floatglass (MIRROTRON Ltd., Hungary) obtained on the GRAINS reflectometer in a cryogenic operating mode of the moderator; data are represented in coordinates Z (detector channel width 0.35 mm) – Time-Of-Flight (channel width 32 μs). b) Reflectivity curves for the same system measured in thermal and cryogenic operating modes of the moderator.

The development and construction of a prototype of a radiography spectrometer on beam 14 (**Fig. 15**) continued.

Fig. 15. Vacuum collimation system (a) and CCD-camera-based imaging system (b).

A vacuum collimation system has been manufactured and installed on the beam. A CCD-camera-based imaging system has been produced and tested on beam 12. The construction of biological shielding of the channel continued. The test opening of a shutter was performed, during which the neutron flux at a sample position was evaluated and found to be $5 \cdot 10^6$ n/cm^2/s.

On the DN-12 diffractometer in cooperation with the Spectrometers' Complex (SC) Department the replacement of detector counters, electronics and data accumulation system has been done. The use of new detectors has made it possible to increase the neutron flux at the instrument by 30%.

After a long break the construction of ZnS-based modules of the ASTRA detector for FSD has been resumed in the SC Department. In cooperation with the specialists from SC a new scintillation

module of the ASTRA detector has been installed and tested in a low-resolution mode on FSD. In the near future this module will be tested in a high-resolution mode. On the FSD diffractometer the tests of a "*List Mode"-analyzer* for accumulation of "raw" data in the list mode continued. The work to develop and improve complex algorithms for recovering high-resolution spectra is in progress.

On the YuMO spectrometer in cooperation with the SC Department the following activities have been carried out: data acquisition electronics of 3 detectors (two ring proportional helium-3 detectors and a direct beam detector) were replaced; gas mixture of the detectors was checked; preamplifiers of ring detectors were replaced, new accumulation electronics were installed, new cables (more than a kilometer in length) from electronics to detectors including vacuum connectors were placed into service. An electronic log and database of experiments were created. The software (including SONIX and SAS) was upgraded.

The technical parameters of the SKAT and EPSILON diffractometers after their modernization have been determined. The values of the neutron flux at a sample position have been estimated using uranium fission chambers and found to be $1.7 \cdot 10^6$ n/cm^2/s for EPSILON and $6.8 \cdot 10^5$ n/cm^2/s for SKAT. Neutron beam profiles have been measured and the resolution function of SKAT has been refined.

To study Li-ion accumulators in real-time diffraction experiments, special model electrochemical cells and temperature control add-on device (**Fig. 16**) which will make it possible to produce temperatures in the range from – 100 to 100 °C (extreme temperature range of operation of accumulators) for a bulky sample have been developed.

a) b)

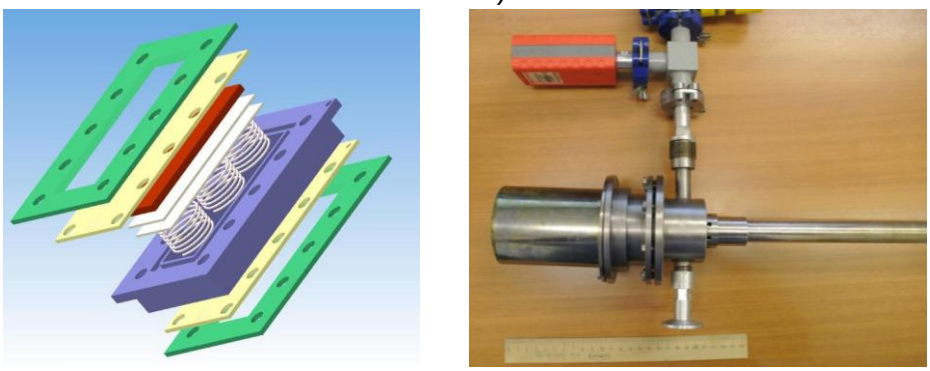

Fig. 16. a) 3D model of a new electrochemical cell for testing electrode materials showing a frame made of corrosion-resistant alloy (green), vanadium current collector plates (yellow), electrode materials (cathode and anode) together with a separator and electrolyte (red), second vanadium current collector, boron nitride and springs (gray), fluoroplastic framing (blue). b) A ready-assembled device for creating special temperature conditions on accumulators.

On the REFLEX reflectometer the investigations of reflectivity properties of thin-film multilayer structures prepared according to a special algorithm proposed by V.K.Ignatovich, have continued (**Fig. 17**) [14].

The idea is to use the properties of certain periodical thin-film structures for designing neutron mirrors with enhanced reflectivity in some definite interval of momentum transfer. Each period consists of a bi-layer with sublayers of positive and negative scattering length density (SLD). Such periodical structure gives a Bragg peak with a height and width determined by SLD values of the sublayers. This approach is an alternative to the widely used technique for producing neutron mirrors with aperiodic structures (magnetron evaporation). This technology does not provide clear scientific criteria for the preparation procedure; the processes are regulated by trial-and-error procedures. This makes the existing method to be unreliable to some extent; it is characterized by a comparatively high

reject rate and long adjustment operations with the equipment. The development of the technology based on a precise mathematical algorithm for constructing neutron mirrors could simplify their design process and improve their quality. Neutron mirrors with high critical angles of total reflection are of current interest for neutron centers engaged in designing neutron guides. The samples for investigations were produced by Mirrotron Ltd, Budapest.

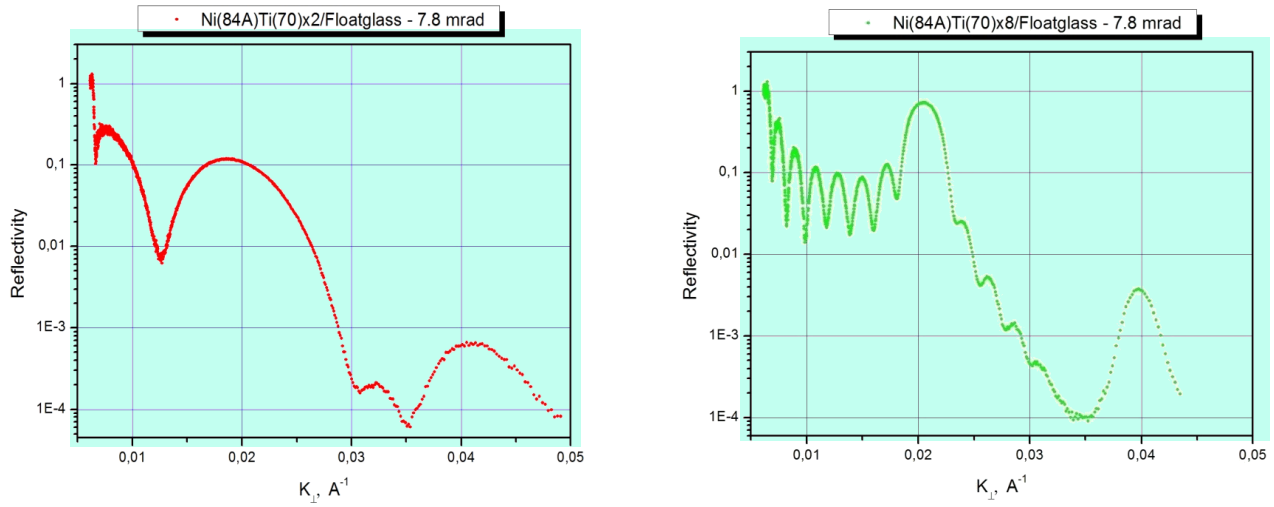

Fig. 17. Reflectivity from periodical structures formed by Ni-Ti bilayers. A scheme at the bottom illustrates the principle of enhanced reflectivity in a wide interval of momentum transfer: sets of bi-layers of various periods form Bragg peaks in a reciprocal space; bi-layer periods are chosen in such a way that peaks overlap and produce a wide interval with high reflectivity.

A technique has been developed for calculating the behavior of the polarization vector of a neutron beam as it passes through magnetic fields of arbitrary spatial configuration. This method allows high-accuracy estimation of losses in the polarization vector value as neutrons pass any spectrometer element, which creates magnetic fields, and thus makes it possible to optimize the instrument. Three-dimensional distributions of magnetic fields from individual elements used on the REFLEX polarized neutron spectrometer on beam 9 of the IBR-2 reactor have been calculated using the MagNet software package. The obtained field distributions were further used by the VITESS software package for simulating changes in the polarization vector.

A study of waveguide layer structure CuNi(15 nm)/$TbCo_5$(150 nm)/CuNi(50 nm)//Si(substrate) has been conducted. Here Cu(33 at.%)Ni(67 at.%) is a nonmagnetic layer and $TbCo_5$ is a weak-magnetic one (saturation magnetization of 500 G) at room temperature. It has been found that changes in magnetization of the order of 10 G can be detected by measuring the intensity of polarized neutron microbeam leaving the end face of the waveguide layer of this structure. Thus, polarized neutron microbeams may be used as a more sensitive method for studying weak-magnetic layers than conventional neutron reflectometry with a sensitivity threshold of the order of 1000 G.

On the REMUR reflectometer a mode of small-angle scattering in grazing incidence geometry has been tested in the framework of planned measurements with a ferromagnetic-superconducting sample. The replacement of motors in the spectrometer drives has been done. For the most part, new software for a 2D position-sensitive detector, which provides data accumulation in four polarization operating modes, has been put into service. Work to design a polarization analyzer with a cross-section of 16 cm × 18 cm is in progress.

References

1. D.P.Kozlenko, S.E.Kichanov, E.V.Lukin, N.T.Dang, L.S.Dubrovinsky, E.A.Bykova,

K.V.Kamenev, H.-P.Liermann, W.Morgenroth, A.Ya.Shapiro, and B. N. Savenko “Effect of high pressure on the crystal structure, magnetic, and vibrational properties of multiferroic $RbFe(MoO_4)_2$”, Phys. Rev. B, v. 87, pp. 014112-1-6 (2013).

2. A.M.Balagurov, I.A.Bobrikov, M.S.Maschenko, D.Sangaa, V.G.Simkin “Structural phase transition in $CuFe_2O_4$ spinel”, Crystallography Reports, v. 58 (5), pp. 710-171 (2013).

3. I.A.Bobrikov, A.M.Balagurov “Real-Time Neutron Diffraction Study of Li-Ion Batteries”, JINR News № 3, p. 19 (2013).

4. E.Burzo, P.Vlaic, D.P.Kozlenko, S.E.Kichanov, N.T.Dang, E.V.Lukin, B.N.Savenko “Magnetic properties of $TbCo_2$ compound at high pressures”, Journal of Alloys and Compounds, v. 551, pp. 702-710 (2013).

5. M.V.Avdeev “Particle interaction in polydisperse magnetic fluids: Experimental aspects of small-angle neutron scattering applications”, Journal of Molecular Liquids (2013), in press.

6. R.A.Eremin, Kh.Kholmurodov, V.I.Petrenko, L.Rosta, M.V.Avdeev. Effect of the solute--solvent interface on small-angle neutron scattering from organic solutions of short alkyl chain molecules as revealed by molecular dynamics simulation. J. Appl. Cryst. v. 46, p. 372-378 (2013).

7. I.V.Gapon, V.I.Petrenko, M.V.Avdeev, L.A.Bulavin, Yu.N.Khaydukov, O.Soltwedel, V.Zavisova, P.Kopcansky, Subtraction of diffuse scattering in analysis of specular neutron reflection at the interface magnetic fluid – silicon, Surface Investigations (2013) accepted.

8. V.I.Petrenko, L.A.Bulavin, M.V.Avdeev, V.M.Garamus, M.Koneracka, P.Kopcansky. Structure and interaction of poly(ethylene glycol) in aqueous solutions. Small-angle neutron scattering data. Macromol. Symposia (2013), accepted.

9. M.V.Avdeev, Aksenov V.L., Tomchuk O.V., Bulavin L.A., Garamus V.M., Osawa E., The spatial diamond–graphite transition in detonation nanodiamond as revealed by small-angle neutron scattering, Journal of Physics: Condensed Matter 25 (2013) P. 445001 (7pp).

10. E.A.Kyzyma, A.A.Tomchuk, L.A.Bulavin, V.I.Petrenko, L.Almasy, M.V.Korobov, D.S.Volkov, I.V.Koshlan, N.A.Koshlan, P.Blyaha, V.L.Aksenov, M.V.Avdeev, Structure and toxicity of aqueous solutions of fullerene C60, Surface Investigations (2013) accepted.

11. M.A. Kiselev, M. Janich, A. Hildebrand, P. Strunz, R.H.H. Neubert, D. Lombardo “Structural transition in aqueous lipid/bile salt [DPPC/NaDC] supramolecular aggregates: SANS and DLS study”, Chem. Phys. v. 424, p. 93-99 (2013).

12. G.E. Iacobescu, M. Balasoiu, I. Bica “Investigation of magnetorheological elastomer surface properties by atomic force microscopy”, Journal of Superconductivity and Novel Magnetism, v. 26, p. 785-792 (2013).

13. J.W.P. Schmelzer, T.V. Tropin “Dependence of the width of the glass transition interval on cooling and heating rates”, J. Chem. Phys., v. 138, p. 034507 (11pp) (2013).

14. T. Veres, L. Cser, V. Bodnarchuck, V. Ignatovich, Z.E. Horváth, B. Nagy “Investigation of periodic Ni–Ti multilayers”, Thin Solid Films, v. 540, p. 69–72 (2013).

15. V.V.Luzin, D.I.Nikolayev, S.Siegizmund. Temperature Induced Internal Stress in Marble, Proc. of the 7th international conference on mechanical stress evaluation by neutron and synchrotron radiation, 10-12 September 2013, Sydney, Australia (in press).